Framework Cu-doped AlPO$_4$ as an effective Fenton-like catalyst for bisphenol A degradation

Lili Zhang [a], Dan Xu [b], Chun Hu [a,c,*], Yilun Shi [d]

[a] Key Laboratory of Drinking Water Science and Technology, Research Center for Eco-Environmental Sciences, Chinese Academy of Sciences, Beijing 100085, China
[b] School of Food and Environment, Dalian University of Technology, Panjin 124221, China
[c] University of Chinese Academy of Sciences, Beijing 100049, China
[d] School of Environmental and Chemical Engineering, Tianjin Polytechnic University, Tianjin 300387, China

ARTICLE INFO

ABSTRACT

Cu-doped AlPO$_4$ molecular sieve was prepared by a hydrothermal method and characterized by field emission scanning electron microscope, X-ray diffraction, extended X-ray absorption fine structure, X-ray photoelectron spectroscopy and nitrogen adsorption/desorption isotherms. The Cu(0.05)-AlPO$_4$ with Cu/Al molar ratio of 0.05 was highly effective and stable for the degradation of bisphenol A (BPA) in the presence of H$_2$O$_2$ at room temperature and neutral pH conditions. The characterization results confirmed that Cu(II)/Cu(I) was co-incorporated into AlPO$_4$ molecular sieve by chemical bonding of Cu—O—T (T for Al or P) in Cu(0.05)-AlPO$_4$, increasing the BET surface area of AlPO$_4$ for more active sites. Excessive copper species existed in the form of Cu(II) and located in the extraframework sites, blocking the porous structure to decrease the specific surface area of AlPO$_4$. The studies of electron spin resonance, *in situ* Raman spectra and other experiments verified that H$_2$O$_2$ was predominately converted into •OH and HO$_2$•/O$_2$•$^-$ in Cu(0.05)-AlPO$_4$ suspension. Specially, the presence of BPA in Cu(0.05)-AlPO$_4$ suspension promoted the convertion of H$_2$O$_2$ into •OH. A mechanism of heterogeneous Fenton catalysis was proposed on the basis of the cycle between Cu(I) and phenoxo-Cu(II) complexes during the interaction of Cu(0.05)-AlPO$_4$, BPA and H$_2$O$_2$.

© 2017 Elsevier B.V. All rights reserved.

1. Introduction

Bisphenol A (BPA) is one of the most common endocrine disruptors, which has been widely used as a raw material for producing polycarbonate plastic, epoxy resins, flame retardants, and other chemical products [1,2]. The global demand for BPA was more than 6.5 million tons in 2012 and its annual growth rate is expected to be 4.6% from 2013 to 2019 [3]. Due to its large production and widespread application, BPA has been released into the aquatic environment by direct discharge of effluents from its manufacture processing, wastewater treatment plants [4] and landfill leachates [5]. The presence of BPA in the aqueous envrionment is harmful to ecosystems and human health. Therefore, it is necessary to develop a proper technique to rapidly and efficiently remove BPA from wastewater, groundwater and even drinking water.

As one of the most effective advanced oxidation processes, Fenton process has unique advantages due to the generation of powerful hydroxyl radical (•OH) by a simple reaction between Fe(II) and H$_2$O$_2$ with low cost and environmental benignity. During this process, most organic pollutants can be nonselectively degraded into non-toxic products under ambient temperature and pressure [6,7]. However, the application of conventional homogeneous Fenton processes is limited by the requirement of low solution pH (<4), the difficulty of Fe^{2+}/Fe^{3+} cycling, and the formation of ferric hydroxide sludge in wastewater treatment [8]. To overcome these problems, the heterogeneous Fenton-like processes have been recently investigated as a more practical and efficient alternative technique for removing recalcitrant organic pollutants over a wider pH range with reduced catalyst loss. Specially, many iron-free catalysts, such as copper [9], Au [10], manganese [11], titanium [12], and carbon materials [13], have sprung up as Fenton-like catalysts to activate H$_2$O$_2$ into reactive oxygen radicals for the degradation of organic pollutants in water.

Among these iron-free catalysts, Cu-containing catalysts have attracted considerable attention in recent years, because of the

high natural abundance and low cost of Cu, and the practical multiple methods to prepare Cu-based materials [14]. In particular, the reduction of Cu^{2+} by H_2O_2 (4.6×10^2 M^{-1} s^{-1}) is more easy than that of Fe^{3+} (0.001–0.02 M^{-1} s^{-1}), and Cu^+ can react efficiently with H_2O_2 to form •OH with a higher reaction rate (1×10^4 M^{-1} s^{-1}) than Fe^{2+} (76 M^{-1} s^{-1}) [15–17]. Due to the mobilization of Cu^{2+}/Cu^+ in water, copper has been suggested to be supported on a porous solid substrate. Cu-containing MFI zeolites [18], Cu/SBA-15 [19], Cu-ZSM-5 [20,21], Cu-impregnated zeolite Y [22] and Cu/TUD-1 [23] have been reported for Fenton-like oxidation of different organic pollutants. The oxidation of organic compounds by the reported Cu-based heterogeneous Fenton-like systems was often followed by the release of Cu (0.5–10 $mg\,L^{-1}$) [24] and the invalid decomposition of H_2O_2 to O_2 [9]. $AlPO_4$ was proven to be a robust support material that produces optimum interactions with metal-based species, facilitating high dispersion and thermal stabilization [25]. Moreover, the incorporation of transition metal cations into the Al and P framework of $AlPO_4$ molecular sieves could markedly enhance the redox catalytic activity [26]. The presence of Cu(I) in the framework of ZSM-5 has been proposed to promote the decomposition of H_2O_2 and the formation of •OH [27]. This paper intends to introduce Cu(I) and Cu(II) into the framework of $AlPO_4$, investigate the performance of Cu-containing $AlPO_4$ for BPA removal through Fenton-like oxidation, and the corresponding •OH formation mechanism by the interaction of BPA with framework Cu(II) and the Cu redox transformation.

In this paper, Cu-doped $AlPO_4$ was prepared, characterized, and assessed for Fenton catalysis. Cu(0.05)-$AlPO_4$ was found to be highly effective and stable for the degradation of BPA at room temperature and neutral pH conditions in the presence of H_2O_2. The possible catalytic mechanism was also discussed.

2. Experimental

2.1. Materials

Copper sulfate ($CuSO_4·5H_2O$), aluminium isopropoxide ($Al(O_iPr)_3$), orthophosphoric acid (H_3PO_4, 85 wt%), diisopropylamine and hydrogen peroxide (H_2O_2, 30%, w/w) were purchased from Sinopharm Chemical Reagent Co., Ltd. 5-Tert-butoxycarbonyl-5-methyl-1-pyrroline-*N*-oxide (BMPO) was provided by Sigma Ltd. Bisphenol A (BPA) was obtained from Acros (Geel, Belgium). All chemicals were at least analytical grade.

2.2. Preparation of catalysts

Cu-doped $AlPO_4$ was synthesized using a hydrothermal method. In a typical procedure, 7.08 g $Al(O_iPr)_3$ was dissolved in 15 mL of deionized water, and stirred at 35 °C for 1 h. Then, 7.4 mL 27.5 wt% H_3PO_4, 5 mL of an aqueous solution containing a certain amount of $CuSO_4·5H_2O$, and 2.5 mL diisopropylamine were added to the $Al(O_iPr)_3$ homogeneous gel in order. Next, the resulting solution was continuously stirred magnetically for 22 h and then transfered to a 50 mL Teflon-lined autoclave and heated in an oven at 180 °C for 72 h. After natural cooling, the obtained solids were filtered, washed with deionized water and dried at 120 °C. The solid product was calcined in air at 550 °C for 8 h. The synthesized samples were denoted as $AlPO_4$, Cu(0.005)-, Cu(0.01)-, Cu(0.015)-, Cu(0.025)-, Cu(0.05)-, Cu(0.075)-, and Cu(0.1)-$AlPO_4$, where the number referred to the Cu/Al molar ratio in the precursor solution (Cu/Al_{pre}) of 0, 0.005, 0.01, 0.015, 0.025, 0.05, 0.075, and 0.1, respectively.

2.3. Characterization

Morphological studies were carried out using a field emission scanning electron microscope (FESEM, Hitachi, S-5500) at acceleration voltage of 5 kV. The crystal structure was analyzed by X-ray diffraction (XRD, Scintag-XDS-2000) equipped with Cu Kα radiation (λ = 1.540598 Å) at 40 kV and 40 mA. X-ray photoelectron spectroscopy (XPS) data were measured on an Kratos AXIS-Ultra instrument with monochromatic Al Kα radiation (225 W, 15 mA, 15 kV) and low-energy electron flooding for charge compensation. The C1 s photoelectron binding energy was set at 284.8 eV and used as reference for calibrating other peak positions. The Fourier transforms of the extended X-ray absorption fine structure (EXAFS) signals were analyzed from Cu K-edge (8.979 keV) X-ray absorption spectra collected at room temperature in transmission mode on the BL14W1 beam line at the Shanghai Synchrotron Radiation Facility (SSRF), China. The background removal, atomic absorption normalization and the EXAFS part extraction were performed using the Winxas 3.1 program. The EXAFS oscillation $\chi(k)$ was extracted using spline smoothing, weighted by k^3 in the high k range, and then transformed to R space with a Hanning function window. The Brunauer-Emmett-Teller (BET) surface area measurements were carried out by N_2 adsorption at 77 K using an ASAP 2020 HD88 instrument. The samples were previously outgassed for 30 min at 150 °C and 4 Pa and then heated for 120 min at 350 °C. For the electron spin resonance (ESR) spectra measurement, 0.01 g of the catalyst was dispersed in 1 mL of water or methanol, following by the addition of 10 μL of H_2O_2 (30%, w/w). Then, 100 μL of the above suspension was quickly mixed with 10 μL of BMPO (250 mM). To test the effect of BPA, 1 mL BPA (100 $mg\,L^{-1}$) with water or methanol as solvent was used to disperse the catalyst. The ESR spectra with BMPO as a spin trap agent were recorded to detect reactive oxygen radicals on a Bruker A300-10/12 ESR spectrometer (microwave frequency: 9.86 GHz; microwave power: 2.29 mW; center field: 3504.07 G; sweep width: 100.00 G; modulation frequency:100.00 kHz; conversion: 80.00 ms; time constant:40.96 ms; and sweep time: 81.92 s). The *in situ* Raman spectra were recorded on a LabRAM HR Evolution (HORIBA, France) equipped with a CCD detector using a laser source at an excitation line of 532 nm. In a typical procedure, 0.05 g of the catalyst was mixed with 3 mL of water or BPA aqueous solution (100 $mg\,L^{-1}$), and then 100 μL of H_2O_2 (30%, w/w) was added. The mixture was placed into the reaction cell, which was scanned from 200 to 2000 cm^{-1}.

2.4. Procedures and analysis

The Fenton-like catalytic experiments were carried out under ambient conditions by using BPA as a model contaminant. In a typical experiment, 1 $g\,L^{-1}$ catalysts were dispersed in the 25 $mg\,L^{-1}$ aqueous solution of BPA (pH 7.0). The mixture was vigorously stirred for 30 min to establish the adsorption/desorption equilibrium. Then, 10 mM H_2O_2 was added into the suspension to initiate the reaction. At fixed time intervals during the degradation process, the analytical samples were taken out and immediately filtered through a 0.22 μm millipore filter to remove the catalyst particles. The solution concentration of BPA was measured by high-performance liquid chromatography (HPLC, 1200 series; Agilent) with an autosampler and a Zorbax SB-Aq column (4.6×250 mm, 5 μm; Agilent), and equipped with an UV detector at the wavelength of 225 nm. The mobile phase was a mixture of 70/30% (v/v) methanol/water and was operated at a flow-rate of 1.0 $mL\,min^{-1}$. The total organic carbon (TOC) was determined by a TOC-V_{CPH} analyzer (Shimadzu) using high-temperature combustion. The metal content in the catalysts after dissolving by nitric acid and hydrofluoric acid and the amount of metallic ions releasing from the
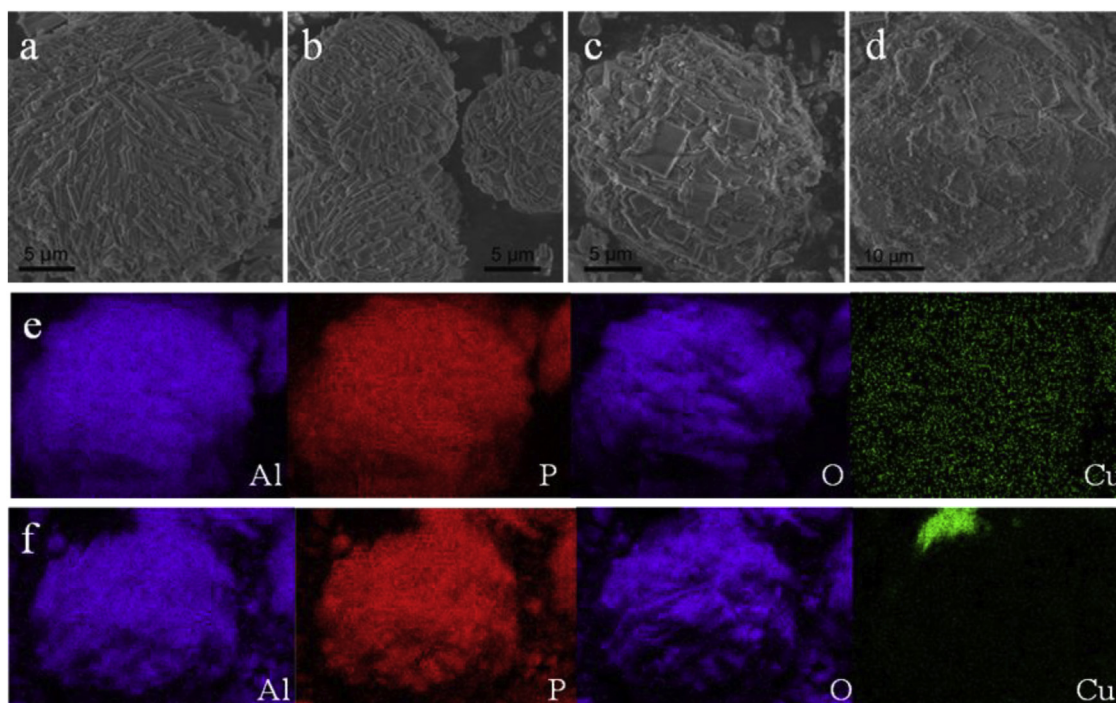
Fig. 1. FESEM images of (a) AlPO$_4$, (b) Cu(0.005)-AlPO$_4$, (c) Cu(0.05)-AlPO$_4$ and (d) Cu(0.075)-AlPO$_4$, and the elemental mappings of (e) Cu(0.05)-AlPO$_4$ and (f) Cu(0.075)-AlPO$_4$.

catalysts during the reaction were measured by inductively coupled plasma optical emission spectrometry (ICP-OES) on an Optima 2000 (PerkinElmer, Inc.). To test the stability and recyclability of Cu(0.05)-AlPO$_4$, the catalyst was filtered, washed with water, and dried at 100 °C. The catalyst was continued to be used in the second cycle. This process was repeated several times.

The utilization efficiency of H$_2$O$_2$ was calculated as follows. In stoichiometry, the complete mineralization of one mole of BPA will consume 36 mol of H$_2$O$_2$ (Eq. (1)).

$$C_{15}H_{16}O_2 + 36H_2O_2 \rightarrow 15CO_2 + 44H_2O \tag{1}$$
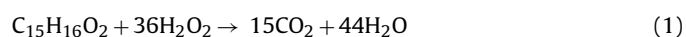
Thus, the utilization efficiency of H$_2$O$_2$ (η) is defined as the ratio of the stoichiometric H$_2$O$_2$ consumption ($[\Delta H_2O_2]_S$) for the mineralization of BPA with the actual H$_2$O$_2$ consumption ($[\Delta H_2O_2]_A$) in the Fenton-like reaction, according to Eq. (2):

$$\eta = [\Delta H_2O_2]_S/[\Delta H_2O_2]_A \tag{2}$$

By measuring the TOC change of the BPA solution, the amount of the mineralized BPA could be obtained, and then the value of $[\Delta H_2O_2]_S$ could be calculated. The actual H$_2$O$_2$ consumption ($[\Delta H_2O_2]_A$) at different reaction time was measured using the potassium titanium (IV) oxalate method [28].

The reported data were the average of the triplicates with a standard deviation of less than 5%.

3. Results and discussion

3.1. Characterization of catalysts

The morphology of AlPO$_4$ and Cu-doped AlPO$_4$ were examined by FESEM. As shown in Fig. 1, AlPO$_4$ particles were composed by the agglomerated rectangular platelets. With increase of Cu contents, the rectangular platelets became shorter and more wide, indicating the crystal growth direction was influenced by Cu doping. In addition, the elemental mappings of Cu(0.05)-AlPO$_4$ confirmed that copper species were highly dispersed into AlPO$_4$ matrix. However, the elemental mappings of Cu(0.075)-AlPO$_4$ revealed the existence

of CuO$_x$ particles or aggregates on the catalyst surface besides part of copper species in AlPO$_4$ matrix.

The XRD patterns of the synthesized samples were shown in Fig. 2. All observed peaks of the AlPO$_4$ and Cu(0.005)-AlPO$_4$ samples can be indexed to a pure orthorhombic AlPO$_4$ phase (JCPDS 47-0599) in Imma space group with lattice parameters $a = 8.10$ Å, $b = 18.01$ Å and $c = 13.82$ Å. With the increase of Cu doping, the crystal phase was gradually transformed to another orthorhombic AlPO$_4$ phase (JCPDS 41-0556) in Icm2 space group with lattice parameters $a = 13.53$ Å, $b = 18.48$ Å and $c = 8.37$ Å, indicating the crystal structure of AlPO$_4$ was interfered by Cu doping. However, the addition of excessive Cu (Cu/Al = 0.075 and 0.1) in the preparation process resulted in the existence of the single phase (JCPDS 47-0599) similar with the undoped AlPO$_4$. For all the Cu-doped samples, no additional peaks attributed to Cu species appeared, suggesting a high dispersion of Cu species in AlPO$_4$ or the existence of amorphous Cu-containing compounds. In addition, the appreciable expansion of the crystal lattice of Cu-doped AlPO$_4$ compared to that of AlPO$_4$ (Table S1) indicated the Cu incorporation into the framework of AlPO$_4$, due to the larger ionic radius of Cu$^+$
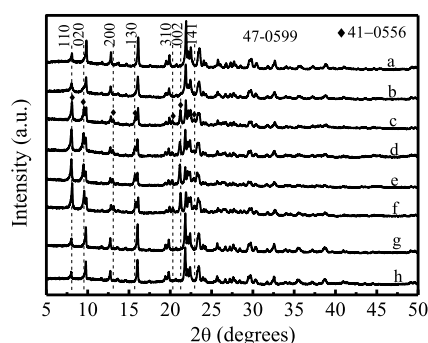

Fig. 2. XRD patterns of Cu-AlPO$_4$ with different Cu/Al mole ratios: (a) Cu/Al = 0, (b) Cu/Al = 0.005, (c) Cu/Al = 0.01, (d) Cu/Al = 0.015, (d) Cu/Al = 0.025, (d) Cu/Al = 0.05, (e) Cu/Al = 0.075, (f) Cu/Al = 0.1.

Table 1
Elemental composition and textural properties of catalysts.

Sample	Cu/Al$_{bulk}$[a]	Cu/Al$_{surf}$[b]	BET surface area
AlPO$_4$	0	–	88.14
Cu(0.005)-AlPO$_4$	0.0037	0.0128	169.00
Cu(0.01)-AlPO$_4$	0.0080	0.0084	175.74
Cu(0.015)-AlPO$_4$	0.0132	–	170.93
Cu(0.025)-AlPO$_4$	0.0182	–	185.30
Cu(0.05)-AlPO$_4$	0.0469	0.0237	104.21
Cu(0.075)-AlPO$_4$	0.0749	0.0446	66.51
Cu(0.1)-AlPO$_4$	0.0929	–	60.92

[a] Bulk Cu/Al molar ratio was obtained by ICP-OES analysis.
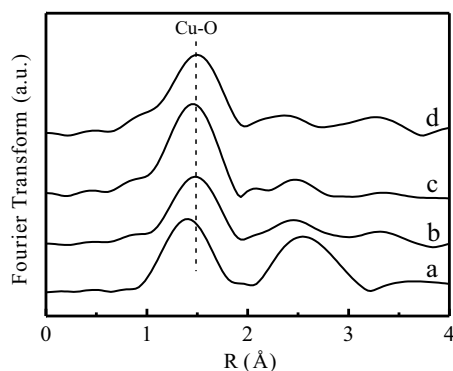[b] Surface Cu/Al molar ratio was obtained by XPS analysis.

Fig. 3. Fourier transforms of Cu K-edge EXAFS for (a) Cu$_2$O, (b) CuO, (c) Cu(0.05)-AlPO$_4$, and (d) Cu(0.075)-AlPO$_4$.

(0.96 Å) and Cu^{2+} (0.72 Å) than that of Al^{3+} (0.51 Å) and P^{5+} (0.34 Å). Therefore, combined with the FESEM results, Cu species dispersely existed in the framework AlPO$_4$ for Cu(0.05)-AlPO$_4$, while amorphous CuO$_x$ clusters existed on the surface of Cu(0.075)-AlPO$_4$ besides part of Cu species in the framework.

Bulk and surface elemental compostition of different samples was analyzed by ICP-OES and XPS, respectively. As shown in Table 1, the bulk Cu/Al molar ratio (Cu/Al$_{bulk}$) of Cu-AlPO$_4$ was slightly lower than Cu/Al$_{pre}$, implying nearly all of the Cu^{2+} precursor could be loaded on AlPO$_4$. The comparison of Cu/Al$_{bulk}$ and Cu/Al$_{surf}$ revealed the heterogeneity of catalysts. For Cu(0.005)-AlPO$_4$, the Cu/Al$_{surf}$ was significantly higher than Cu/Al$_{bulk}$. The diversity between Cu/Al$_{surf}$ and Cu/Al$_{bulk}$ was subtle for Cu(0.01)-AlPO$_4$. And the Cu/Al$_{surf}$ was significantly lower than Cu/Al$_{bulk}$ for Cu(0.05)-AlPO$_4$ and Cu(0.075)-AlPO$_4$. The metal states in the samples with different Cu contents were further studied by EXAFS. Fig. 3 showed the Fourier transform of the EXAFS data for the different samples. The first peak in the Fourier Transform could be assigned to the Cu—O shell [29]. Specially, for Cu(0.05)-AlPO$_4$, the Cu—O shell was located at 1.45 Å, which was shorter than that in CuO (1.48 Å) and longer than that in Cu$_2$O (1.41 Å), indicating that the Cu existed mostly as isolated Cu species in the framework of AlPO$_4$ rather than CuO or Cu$_2$O particles [30]. The second peak was a composite peak, possibly including a combination of Cu···T and Cu–Cu [31]. Distinguishing P from Al by EXAFS was impossible due to the almost identical backscattered waves, thus T was used to designate both Al and P [32]. For Cu(0.075)-AlPO$_4$, the two peaks were similar with CuO, suggesting the formation of CuO clusters in Cu(0.075)-AlPO$_4$.

As shown in Fig. 4, the Cu2p$_{3/2}$ peak of Cu(0.005)-AlPO$_4$ was at 933.2 eV for Cu$^+$, confirming by the auger parameters at 1847.4 eV based on the AES measurements. For the Cu(0.01, 0.05, 0.075)-AlPO$_4$ samples, the Cu 2p$_{3/2}$ spectra can be fitted into two peaks with binding energies at 933.2 eV and 935.2 eV, corresponding to Cu$^+$ and Cu^{2+}. The additional shake-up satellite peak around 943.5 eV implied the presence of an unfilled Cu 3d^9 shell and thus further confirming the existence of Cu(II) on the surface of these samples [33]. Moreover, the Cu(I) to Cu(II) atomic ratios on the surface of Cu(0.01, 0.05, 0.075)-AlPO$_4$ were 3.17:1, 2.57:1, and 2.12:1, respectively, indicating that the atomic percentage of Cu(I) decreased with the increase of Cu doping in AlPO$_4$. The phenomenon that different Cu doping would lead to different Cu species were also observed in Cu-doped γ-Al$_2$O$_3$ material by Fu et al. [34]. In order to neutralize local background, the chemical state of Cu species was reduced at low doping level since three
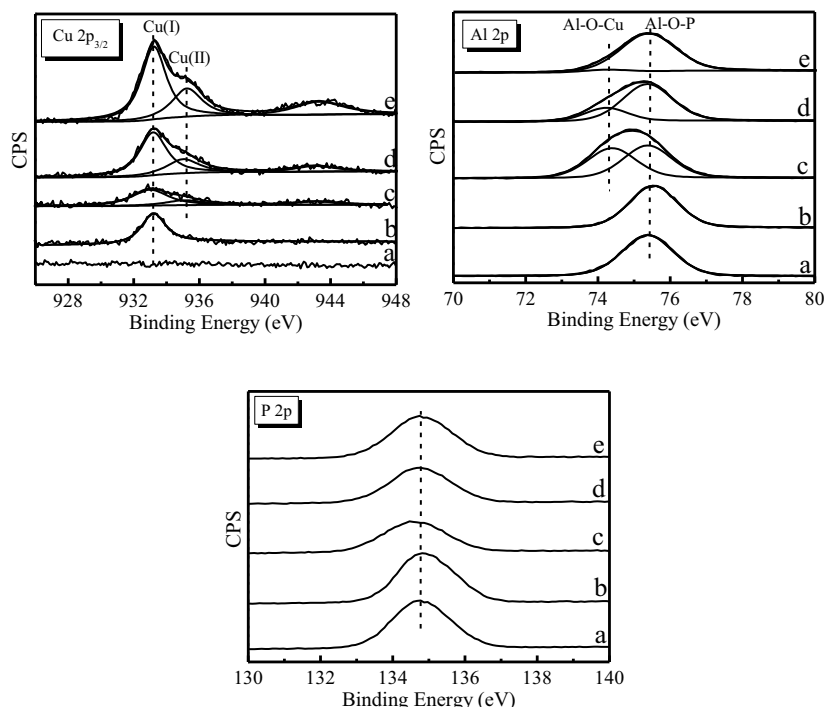

Fig. 4. XPS spectra of (a) AlPO$_4$, (b) Cu(0.005)-AlPO$_4$, (c) Cu(0.01)-AlPO$_4$, (d) Cu(0.05)-AlPO$_4$, and (e) Cu(0.075)-AlPO$_4$.
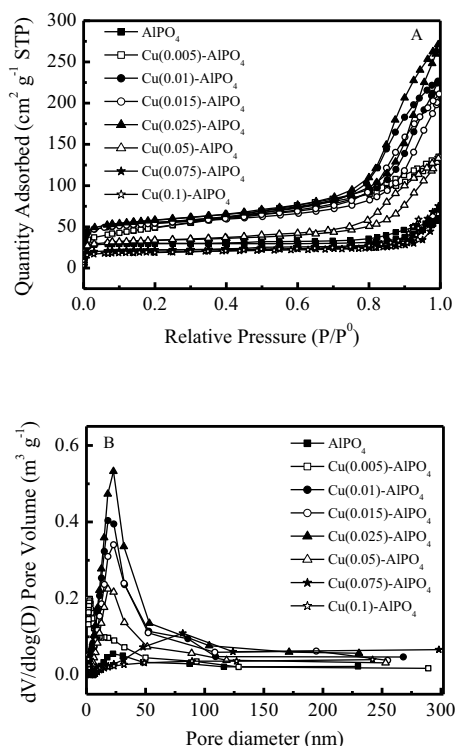
Fig. 5. (A) N_2 adsorption/desorption isotherms and (B) pore-size distribution curves of different samples.

Fig. 6. Effect of the Cu/Al mole ratios of Cu-AlPO$_4$ (1.0 g L^{-1}) on (A) BPA (25 mg L^{-1}) degradation, (B) TOC removal and (C) releasing of Cu during the BPA degradation in the corresponding suspensions with H$_2$O$_2$ (10 mM) at pH 7: (a) Cu/Al=0, (b) Cu/Al=0.005, (c) Cu/Al=0.01, (d) Cu/Al=0.015, (e) Cu/Al=0.025, (f) Cu/Al=0.05, (g) Cu/Al=0.075, (h) Cu/Al=0.1.

electrons were introduced by Al and five electrons were introduced by P, but further oxidized at higher doping level partly because of the increase of the extraframework Cu. The Al2p peaks of AlPO$_4$ and Cu(0.005)-AlPO$_4$ were at 75.4 eV for Al^{3+} in Al—O—P. For Cu(0.01, 0.05)-AlPO$_4$, the Al2p spectra can be fitted into two peaks with binding energies at 74.3 eV and 75.4 eV, assigned to Al^{3+} in Al—O—Cu and Al-O-P, respectively [35], while Al mainly existed in Al-O-P for Cu(0.075)-AlPO$_4$ since the signal for Al^{3+} in Al—O—Cu was very small. Similarly, the P2p peaks of AlPO$_4$ and Cu(0.005)-AlPO$_4$ were at 134.8 eV for P^{5+} in Al-O-P, while a composite peak was observed for Cu(0.01, 0.05, 0.075)-AlPO$_4$, probably including P^{5+} in Cu-O-P and Al-O-P, respectively. These results suggested that Cu mainly incorporated in the framework of AlPO$_4$ for Cu(0.005, 0.01, 0.05)-AlPO$_4$, in line with the results of XRD and EXAFS analysis. For Cu(0.075)-AlPO$_4$, most of the Cu species were in the extraframework, consistent with the results of FESEM and EXAFS, and some Cu species existed in the framework as evidenced by the expansion of crystal lattice after Cu doping (Table S1).

The N$_2$ adsorption/desorption isotherms of the AlPO$_4$ and Cu-AlPO$_4$ samples were shown in Fig. 5. All the samples exhibited type IV isotherms with H3 hysteresis loops, characteristic of a solid mesoporous structure with the existence of slit-like pores. Compared with AlPO$_4$, the appropriate doping of Cu led to higher absorption at a relative pressure around 0.75–1, suggesting the presence of more mesopores in Cu-AlPO$_4$, which was also demonstrated by the pore-size distribution curves (Fig. 5B). However, excessive doping of Cu in AlPO$_4$ resulted in the reduction of mesopores. The pore structure of AlPO$_4$ and Cu(0.005-0.05)-AlPO$_4$ was basically mesoporous with a narrow pore size distribution centered at about 25 nm due to the pores formed in the interior part of AlPO$_4$, while more large mesopores existed in Cu(0.075)-AlPO$_4$ with a wide pore-size distribution range centered at over 80 nm ascribed to the pores formed between the particles [36] and no pores less than 250 nm were observed in Cu(0.1)-AlPO$_4$. As shown in Table 1, the appropriate doping of Cu significantly increased the BET sur-
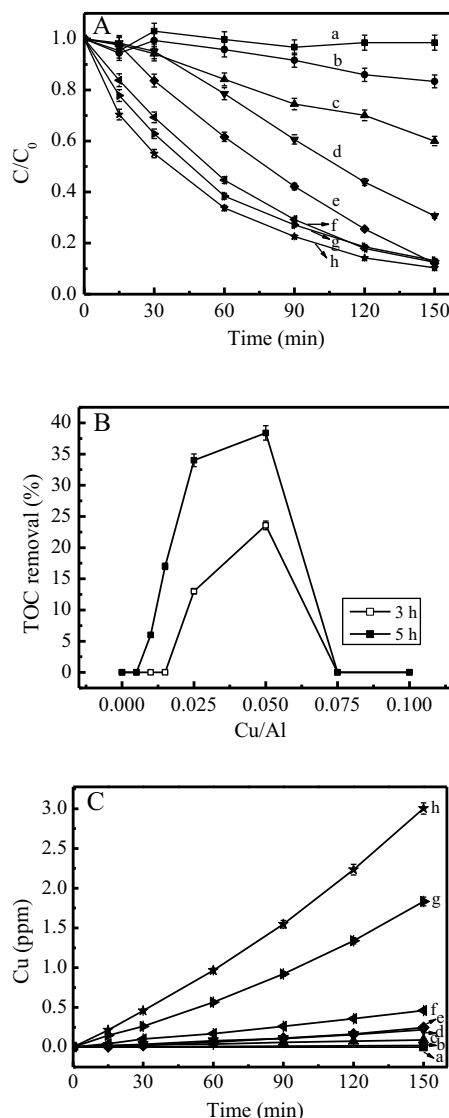
face area of AlPO$_4$ from 88.14 m^2 g^{-1} for AlPO$_4$ to 185.30 m^2 g^{-1} for Cu(0.025)-AlPO$_4$, and the BET surface area of Cu(0.05)-AlPO$_4$ (104.21 m^2 g^{-1}) was smaller than that of Cu(0.025)-AlPO$_4$, but still larger than that of the undoped AlPO$_4$, indicating the Cu incorporation into the framework of AlPO$_4$ without blocking of the porous structure. However, the excessive doping of Cu decreased the BET surface area for Cu(0.075, 0.1)-AlPO$_4$, indicating the formation of the extraframework Cu species plugging the porous structure.

3.2. Catalytic degradation of BPA in Cu-AlPO$_4$ suspension with H$_2$O$_2$

AlPO$_4$ and Cu-AlPO$_4$ were applied for the catalytic removal of BPA in the presence of H$_2$O$_2$ at room temperature and neutral pH. The effect of Cu doping on the activity of catalysts was shown in Fig. 6A. No significant degradation of BPA was observed in AlPO$_4$ suspension. With the increase of Cu doping in AlPO$_4$, the degradation rate of BPA gradually increased and up to 88% of BPA was removed within 150 min for Cu(0.05)-
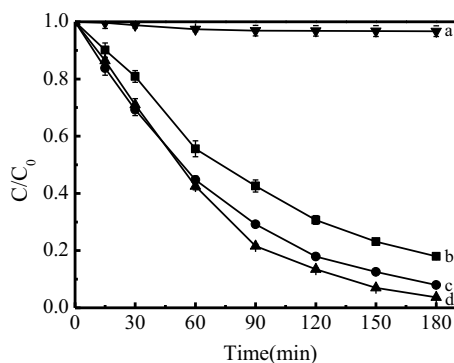
Fig. 7. Effect of catalyst concentration on BPA ($25 \, mg \, L^{-1}$) degradation in the Cu(0.05)-AlPO$_4$ suspension with H$_2$O$_2$ (10 mM): (a) in the absence of catalyst; (b) $0.5 \, g \, L^{-1}$ catalyst; (c) $1.0 \, g \, L^{-1}$ catalyst; and (d) $1.5 \, g \, L^{-1}$ catalyst.

Fig. 8. Effect of H$_2$O$_2$ dosage on BPA ($25 \, mg \, L^{-1}$) degradation in the Cu(0.05)-AlPO$_4$ suspension ($1.0 \, g \, L^{-1}$): (a) 0 mM H$_2$O$_2$; (b) 5 mM H$_2$O$_2$; (c) 10 mM H$_2$O$_2$; (d) 15 mM H$_2$O$_2$; (e) 20 mM H$_2$O$_2$; (f) 25 mM H$_2$O$_2$; and (g) 30 mM H$_2$O$_2$.

AlPO$_4$. With a higher Cu/Al molar ratio of 0.075 and 0.1, the degradation of BPA was not significantly increased. Correspondingly, Cu(0.05)-AlPO$_4$ exhibited the highest TOC removal rate (Fig. 6B). Note that no significant TOC removal was observed in Cu(0.075, 0.1)-AlPO$_4$ suspensions with H$_2$O$_2$, implying the important role of framework Cu in the high activity of catalysts. During BPA degradation, the concentration of dissolved metals was determined in Fig. 6C. After 150 min reaction, the amount of Cu release followed the order of AlPO$_4$ ($0 \, mg \, L^{-1}$) < Cu(0.005)-AlPO$_4$ ($0.022 \, mg \, L^{-1}$) < Cu(0.01)-AlPO$_4$ ($0.091 \, mg \, L^{-1}$) < Cu(0.015)-AlPO$_4$ ($0.219 \, mg \, L^{-1}$) < Cu(0.025)-AlPO$_4$ ($0.248 \, mg \, L^{-1}$) < Cu(0.05)-AlPO$_4$ ($0.461 \, mg \, L^{-1}$) < Cu(0.075)-AlPO$_4$ ($1.834 \, mg \, L^{-1}$) < Cu(0.1)-AlPO$_4$ ($3.003 \, mg \, L^{-1}$), suggesting that there existed an optimal Cu/Al molar ratio in the preparation process for the stability of Cu-AlPO$_4$. According to the characterization results, Cu species were mainly in the framework of Cu(0.005-0.05)-AlPO$_4$, while most of the Cu species were in the extraframework of Cu(0.075-0.1)-AlPO$_4$. Thus, the framework Cu species were more stable than the extraframework Cu species during the Fenton-like reaction. The slightly high reactivity of Cu(0.075)-AlPO$_4$ and Cu(0.1)-AlPO$_4$ to the degradation of BPA substrate was mainly due to the catalytic contribution of released ions. Under the same reaction conditions (*i.e.*, initial pH 7, initial BPA concentration $25 \, mg \, L^{-1}$, initial H$_2$O$_2$ concentration 10 mM), 69% and 75% of BPA can be degraded within 150 min in the presence of $1.834 \, mg \, L^{-1}$ and $3.003 \, mg \, L^{-1}$ Cu^{2+}, respectively. And no TOC removal was observed after 5 h reaction in $1.834 \, mg \, L^{-1}$ or $3.003 \, mg \, L^{-1}$ Cu^{2+} solution with H$_2$O$_2$. The activity of the Cu(0.05)-AlPO$_4$ catalyst during successive runs was performed and shown in Fig. S1. The cycle tests exhibited that the conversion of BPA decreased by 9% in the fifth cycle of Cu(0.05)-AlPO$_4$ and remained at approximately 83% within 180 min in the continuous cycles. The results indicated that Cu(0.05)-AlPO$_4$ had an excellent stability. In addition, the surface concentration ratio of Cu$^+$ to Cu^{2+} was approximately 0.48:1 on the surface of Cu(0.05)-AlPO$_4$ after 1 h of reaction, which was less than the 2.57:1 ratio prior to the reaction. The Cu$^+$ to Cu^{2+} ratio returned to 2.44:1 after 24 h of reaction based on XPS analysis (Fig. S2). The results suggested that the Cu redox transformation occurred between Cu$^+$ and Cu^{2+} species. Therefore, the high activity and stability of Cu(0.05)-AlPO$_4$ were probably related to its large surface area and the existence of framework Cu(II)/Cu(I).

The effect of the Cu(0.05)-AlPO$_4$ catalyst concentration on the activity was investigated in Fig. 7. In the absence of catalyst, no significant degradation of BPA was observed. The degradation efficiency improved with the increasing catalyst concentration, and about 82% and 92% of BPA were degraded within 180 min at a catalyst concentration of $0.5 \, g \, L^{-1}$ and $1.0 \, g \, L^{-1}$, respectively. A higher concentration of $1.5 \, g \, L^{-1}$ did not cause much improvement of the
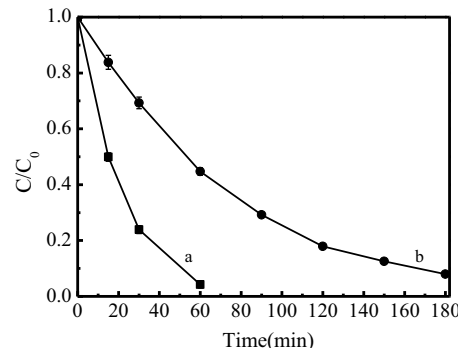

Fig. 9. The degradation of BPA with different initial concentrations in the Cu(0.05)-AlPO$_4$ suspension ($1.0 \, g \, L^{-1}$) with H$_2$O$_2$ (10 mM): (a) $10 \, mg \, L^{-1}$ and (b) $25 \, mg \, L^{-1}$.

degradation efficiency. Meanwhile, the influence of H$_2$O$_2$ concentration was further explored at a catalyst concentration of $1.0 \, g \, L^{-1}$. As shown in Fig. 8, only 6% of BPA was degraded in the absence of H$_2$O$_2$ even after 180 min reaction. The BPA degradation was significantly promoted in the presence of H$_2$O$_2$. Catalytic degradation of up to 92% was observed with 10 mM H$_2$O$_2$ added within 180 min. Further increase of H$_2$O$_2$ concentration to 25 mM did not result in an obviously improved efficiency. Excessive H$_2$O$_2$ dosage (*e.g.* 30 mM) resulted in a slight decrease of BPA degradation due to an invalid decomposition of H$_2$O$_2$ from its own scavenging effect. In addition, the effect of the initial BPA concentration on its degradation by Cu(0.05)-AlPO$_4$ was determined as shown in Fig. 9. At a relative lower concentration of $10 \, mg \, L^{-1}$, almost all of BPA was completely removed within 60 min, indicating Cu(0.05)-AlPO$_4$ can accelerate the degradation of pollutants with lower concentration.

According to the previously described method [37], the utilization efficiency of H$_2$O$_2$ (η) is defined as the ratio of the stoichiometric H$_2$O$_2$ consumption ($[\Delta H_2O_2]_S$) for the mineralization of pollutants with the actual H$_2$O$_2$ consumption ($[\Delta H_2O_2]_A$) in the Fenton reaction. As shown in Table 2, the utilization efficiency of H$_2$O$_2$ was maintained at about 50% during the reaction, which was comparable to that of the reported Cu-based systems.

Table 2
Actual H$_2$O$_2$ consumption ($[\Delta H_2O_2]_A$) and stoichiometric H$_2$O$_2$ consumption ($[\Delta H_2O_2]_S$) for mineralizing BPA ($25 \, mg \, L^{-1}$) during the Fenton-like reaction.

Reaction Time/h	$[\Delta H_2O_2]_A$/mM	$[\Delta H_2O_2]_S$/mM	η
0	0	0	–
48	4.74	2.64	0.56
72	5.72	2.79	0.49
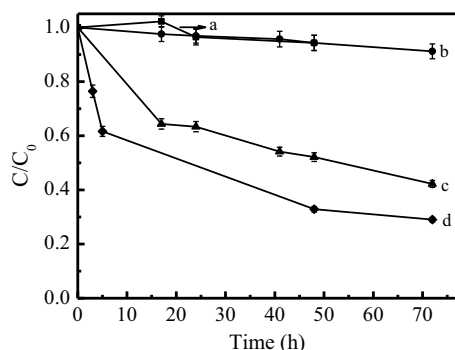
Fig. 10. The decomposition of H_2O_2 in (a) BPA, (b)H_2O + Cu(0.05)-AlPO$_4$, and (c) BPA + Cu(0.05)-AlPO$_4$; (d) TOC removal in Cu(0.05)-AlPO$_4$ suspension with H_2O_2. (Initial pH 7, initial BPA concentration 25 mg L^{-1}, initial H_2O_2 concentration 10 mM, catalyst concentration 1.0 g L^{-1}).
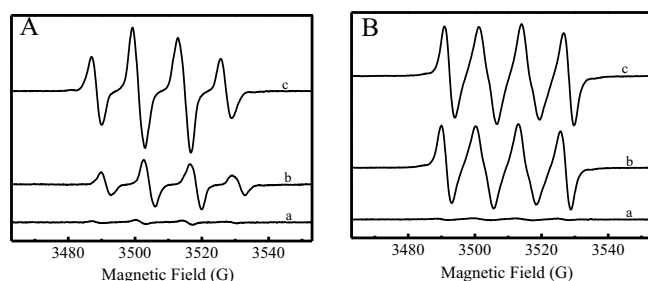

Fig. 12. *In situ* Raman spectra for various catalyst aqueous dispersions: (a) AlPO$_4$; (b) AlPO$_4$ + H_2O_2; (c) Cu(0.05)-AlPO$_4$; (d) Cu(0.05)-AlPO$_4$ + BPA; (e) Cu(0.05)-AlPO$_4$ + H_2O_2; and (f) Cu(0.05)-AlPO$_4$ + BPA + H_2O_2.

Fig. 11. BMPO spin trapping ESR spectra recorded at ambient temperature (A) in aqueous dispersion for BMPO-•OH and (B) in methanol dispersion for BMPO-HO$_2$•/O$_2$•$^-$: (a) H_2O_2 + BMPO; (b) Cu(0.05)-AlPO$_4$ + H_2O_2 + BMPO; and (c) Cu(0.05)-AlPO$_4$ + BPA + H_2O_2 + BMPO.

3.3. Reaction mechanism

As shown in Fig. 10, almost no decomposition of H_2O_2 (10 mM) was observed in BPA without catalysts. Its decomposition was also not significant in Cu(0.05)-AlPO$_4$ without organic compounds. However, the presence of the substrate BPA in Cu(0.05)-AlPO$_4$ suspension obviously increased the decomposition of H_2O_2. These results suggested that the interaction between Cu(0.05)-AlPO$_4$ and BPA promoted the decomposition of H_2O_2.

To further ascertain the reaction mechanism, the reactive oxygen radicals in different catalyst suspensions were detected by the ESR spin-trapping technique. As shown in Fig. 11, no significant signals were attributed to reactive oxygen radicals in the control experiments, while four characteristic peaks of BMPO-•OH were observed in the suspension of Cu(0.05)-AlPO$_4$ with H_2O_2. It's worth noting that the intensities of the signals significantly increased in the presence of BPA. The formation of HO$_2$•/O$_2$•$^-$ radicals was also detected in methanol (Fig. 11B), since the HO$_2$•/O$_2$•$^-$ radicals in water were very unstable and underwent facile disproportionation. The characteristic peaks of BMPO-HO$_2$•/O$_2$•$^-$ adducts were observed in Cu(0.05)-AlPO$_4$ suspension with H_2O_2, and the intensities of the signals were not significantly changed in the presence of BPA. The results of H_2O_2 decomposition and ESR analysis confirmed that the interaction between Cu(0.05)-AlPO$_4$ and BPA promoted the decomposition of H_2O_2 into •OH.

In addition, the interaction processes of the corresponding samples with H_2O_2 were observed by *in situ* Raman spectroscopy (Fig. 12). No significant peaks appeared in the suspension of AlPO$_4$ with and without H_2O_2 (curve a and b). For Cu(0.05)-AlPO$_4$, only the system Raman bands could be observed with and without BPA before adding H_2O_2 (curve c and d). However, a band located at 876 cm^{-1} appeared upon addition of H_2O_2 to the suspension of
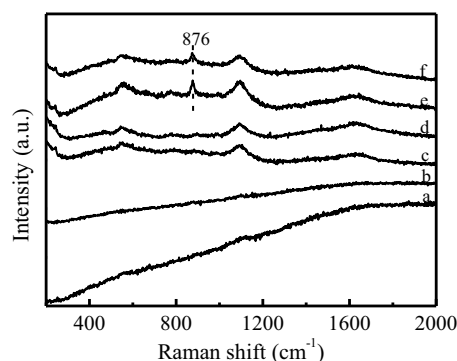
Cu(0.05)-AlPO$_4$ (curve e). According to previous studies [38,39], Cu(II) and H_2O_2 could form transient complexes, and the absorption band was assigned to the O—O stretching of peroxo complexes formed on Cu^{2+} sites of Cu(0.05)-AlPO$_4$. Specially, the above absorption band decreased in the presence of BPA (curve f). As previously reported, the surface Cu(II) species of Cu(0.05)-AlPO$_4$ could form phenoxo-Cu(II) complexes with BPA and its intermediates by σ bonding [40], and orbital interactions involving electron transfer of the type π → Cu(II) (σ donation) were possible and would improve the electronic polarity of the benzene ring in the phenoxo-Cu(II) complexes [41]. Therefore, the formation of phenoxo-Cu(II) complexes could cause the reaction of the organic ligand part with the activated H_2O_2, and during this process, Cu(II) in the phenoxo-Cu(II) complexes would get an electron due to the charge transfer from the benzene ring to Cu(II) by the π → Cu(II) interation, leading to the reduction of Cu(II) to Cu(I) and the accelerated decomposition of H_2O_2 into more •OH.

According to the above results, a possible interaction process among the framework copper species of Cu-AlPO$_4$, BPA and H_2O_2 was proposed during the Fenton-like catalytic degradation of BPA. On the one hand, H_2O_2 was reduced by Cu(I) to generate •OH and Cu(II) [42]. On the other hand, the direct reaction of H_2O_2 and the phenoxo-Cu(II) complexes facilitated the reduction of Cu(II) to Cu(I) and the effective decomposition of H_2O_2 into •OH on the catalyst surface, resulting in the high activity of Cu(0.05)-AlPO$_4$.

4. Conclusions

Cu-doped AlPO$_4$ molecular sieve with Cu/Al molar ratio of 0.05 exhibited high activity and stability for the degradation of BPA with H_2O_2 at room temperature and neutral pH conditions. •OH and HO$_2$•/O$_2$•$^-$ radicals were the main active species in the reaction by the studies of ESR. Cu(II)/Cu(I) was confirmed to be coexisted in the framework structure of AlPO$_4$ and the BET surface area was increased for more active sites. Cu(I) was Fenton active to reduce H_2O_2 into •OH, and Cu(II) chelated with BPA or its intermediates could react with H_2O_2 to form more •OH, resulting in the high Fenton catalytic activity.

Appendix A. Supplementary data

Supplementary data associated with this article can be found, in the online version, at http://dx.doi.org/10.1016/j.apcatb.2017.02.002.

References

[1] J. Du, J. Bao, X. Fu, C. Lu, S.H. Kim, Mesoporous sulfur-modified iron oxide as an effective Fenton-like catalyst for degradation of bisphenol A, Appl. Catal. B: Environ. 184 (2016) 132–141.

[2] S. Li, G. Zhang, P. Wang, H. Zheng, Y. Zheng, Microwave-enhanced Mn-Fenton process for the removal of BPA in water, Chem. Eng. J. 294 (2016) 371–379.

[3] J. Im, F.E. Löffler, Fate of bisphenol A in terrestrial and aquatic environments, Environ. Sci. Technol. 50 (2016) 8403–8416.

[4] L. Yang, Z. Li, H. Jiang, W. Jiang, R. Su, S. Luo, Y. Luo, Photoelectrocatalytic oxidation of bisphenol A over mesh of TiO₂/graphene/Cu₂O, Appl. Catal. B: Environ. 183 (2016) 75–85.

[5] Y. Kalmykova, K. Björklund, A.M. Strömvall, L. Blom, Partitioning of polycyclic aromatic hydrocarbons alkylphenols, bisphenol A and phthalates in landfill leachates and stormwater, Water Res. 47 (2013) 1317–1328.

[6] A.D. Bokare, W. Choi, Review of iron-free Fenton-like systems for activating H₂O₂ in advanced oxidation processes, J. Hazard. Mater. 275 (2014) 121–135.

[7] S. Yuan, X. Mao, A.N. Alshawabkeh, Efficient degradation of TCE in groundwater using Pd and electro-generated H₂ and O₂: a shift in pathway from hydrodechlorination to oxidation in the presence of ferrous ions, Environ. Sci. Technol. 46 (2012) 3398–3405.

[8] M. Wang, G. Fang, P. Liu, D. Zhou, C. Ma, D. Zhang, J. Zhan, Fe₃O₄@β-CD nanocomposite as heterogeneous Fenton-like catalyst for enhanced degradation of 4-chlorophenol (4-CP), Appl. Catal. B: Environ. 188 (2016) 113–122.

[9] Y. Zhang, C. Liu, B. Xu, F. Qi, W. Chu, Degradation of benzotriazole by a novel Fenton-like reaction with mesoporous Cu/MnO₂: combination of adsorption and catalysis oxidation, Appl. Catal. B: Environ. 199 (2016) 447–457.

[10] X. Yang, P. Tian, C. Zhang, Y. Deng, J. Xu, J. Gong, Y. Han, Au/carbon as Fentonlike catalysts for the oxidative degradation of bisphenol A, Appl. Catal. B: Environ. 134 (2013) 145–152.

[11] J. Zbiljic, O. Vajdle, V. Guzsvany, J. Molnar, J. Agbaba, B. Dalmacija, K. Kalcher, Hydrodynamic chronoamperometric method for the determination of H₂O₂ using MnO₂-based carbon paste electrodes in groundwater treated by Fenton and Fenton-like reagents for natural organic matter removal, J. Hazard. Mater. 283 (2015) 292–301.

[12] D. Wiedmer, E. Sagstuen, K. Welch, H.J. Haugen, H. Tiainen, Oxidative power of aqueous non-irradiated TiO₂-H₂O₂ suspensions: methylene blue degradation and the role of reactive oxygen species, Appl. Catal. B: Environ. 198 (2016) 9–15.

[13] M.T. Pinho, H.T. Gomes, R.S. Ribeiro, J.L. Faria, A.M.T. Silva, Carbon nanotubes as catalysts for catalytic wet peroxide oxidation of highly concentrated phenol solutions: towards process intensification, Appl. Catal. B: Environ. 165 (2015) 706–714.

[14] M.B. Gawande, A. Goswami, F. Felpin, T. Asefa, X. Huang, R. Silva, X. Zou, R. Zboril, R.S. Varma, Cu and Cu-based nanoparticles: synthesis and applications in catalysis, Chem. Rev. 116 (2016) 3722–3811.

[15] D.A. Nichela, A.M. Berkovic, M.R. Costante, M.P. Juliarena, F.S.G. Einschlag, Nitrobenzene degradation in Fenton-like systems using Cu(II) as catalyst. Comparison between Cu(II)- and Fe(III)-based systems, Chem. Eng. J. 228 (2013) 1148–1157.

[16] M.K. Eberhardt, G. Ramirez, E. Ayala, Does the reaction of Cu⁺ with H₂O₂ give OH radicals? A study of aromatic hydroxylation, J. Org. Chem. 54 (1989) 5922–5926.

[17] J.F. Perez-Benito, Reaction pathways in the decomposition of hydrogen peroxide catalyzed by copper(II), J. Inorg. Biochem. 98 (2004) 430–438.

[18] O.P. Taran, S.A. Yashnik, A.B. Ayusheev, A.S. Piskun, R.V. Prihod'ko, Z.R. Ismagilov, V.V. Goncharuk, Cu-containing MFI zeolites as catalysts for wet peroxide oxidation of formic acid as model organic contaminant, Appl. Catal. B: Environ. 140–141 (2013) 506–515.

[19] V. Subbaramaiah, V.C. Srivastava, I.D. Mall, Optimization of reaction parameters and kinetic modeling of catalytic wet peroxidation of picoline by Cu/SBA-15, Ind. Eng. Chem. Res. 52 (2013) 9021–9029.

[20] O.P. Taran, A.N. Zagoruiko, A.B. Ayusheev, S.A. Yashnik, R.V. Prihod'ko, Z.R. Ismagilov, V.V. Goncharuk, V.N. Parmon, Wet peroxide oxidation of phenol over Cu-ZSM-5 catalyst in a flow reactor. Kinetics and diffusion study, Chem. Eng. J. 282 (2015) 108–115.

[21] S. Jiang, H. Zhang, Y. Yan, Catalytic wet peroxide oxidation of phenol wastewater over a novel Cu-ZSM-5 membrane catalyst, Catal. Commun. 71 (2015) 28–31.

[22] L. Singh, P. Rekha, S. Chand, Cu-impregnated zeolite Y as highly active and stable heterogeneous Fenton-like catalyst for degradation of Congo red dye, Sep. Purif. Technol. 170 (2016) 321–336.

[23] M.P. Pachamuthu, S. Karthikeyan, R. Maheswari, A.F. Lee, A. Ramanathan, Fenton-like degradation of Bisphenol A catalyzed by mesoporous Cu/TUD-1, Appl. Surf. Sci. 393 (2017) 67–73.

[24] Y.H. Ling, M.C. Long, P.D. Hu, Y. Chen, J.W. Huang, Magnetically separable core–shell structural γ-Fe₂O₃@Cu/Al-MCM-41 nanocomposite and its performance in heterogeneous Fenton catalysis, J. Hazard. Mater. 264 (2014) 195–202.

[25] M. Machida, S. Minami, K. Ikeue, S. Hinokuma, Y. Nagao, T. Sato, Y. Nakahara, Rhodium nanoparticle anchoring on AlPO₄ for efficient catalyst sintering suppression, Chem. Mater. 26 (2014) 5799–5805.

[26] M. Machida, S. Minami, S. Hinokuma, H. Yoshida, Y. Nagao, T. Sato, Y. Nakahara, Unusual redox behavior of Rh/AlPO₄ and its impact on three-way catalysis, J. Phys. Chem. C 119 (2015) 373–380.

[27] X. Zhou, H. Chen, X. Cui, Z. Hua, Y. Chen, Y. Zhu, Y. Song, Y. Gong, J. Shi, A facile one-pot synthesis of hierarchically porous Cu(I)-ZSM-5 for radicals-involved oxidation of cyclohexane, Appl. Catal. A: Gen. 451 (2013) 112–119.

[28] R.M. Sellers, Spectrophotometric determination of hydrogen peroxide using potassium titanium (IV) oxalate, Analyst 105 (1980) 950–954.

[29] L.E. Gómez, B.M. Sollier, M.D. Mizrahi, J.M.R. López, E.E. Miró, A.V. Boix, Preferential CO oxidation on Pt-Cu/Al₂O₃ catalysts with low Pt loadings, Int. J. Hydrogen Energy 39 (2014) 3719–3729.

[30] M.K. Neylon, C.L. Marshall, A. Jeremy Kropf, In situ EXAFS analysis of the temperature-programmed reduction of Cu-ZSM-5, J. Am. Chem. Soc. 124 (2002) 5457–5465.

[31] K. Mathisen, D.G. Nicholson, A.M. Beale, M. Sanchez-Sanchez, G. Sankar, W. Bras, S. Nikitenko, Comparing CuAPO-5 with Cu:ZSM-5 in the selective catalytic reduction of NOₓ: an in situ study, J. Phys. Chem. C 111 (2007) 3130–3138.

[32] K. Mathisen, D.G. Nicholson, A.N. Fitch, M. Stockhuber, Selective catalytic reduction of NOₓ over microporous CuAPO-5: structural characterisation by XAS and XRD, J. Mater. Chem. 15 (2005) 204–217.

[33] F.E. López-Suárez, A. Bueno-López, M.J. Illán-Gómez, A. Adamski, B. Ura, J. Trawczynski, Copper ctalysts for soot oxidation: alumina versus perovskite supports, Environ. Sci. Technol. 42 (2008) 7670–7675.

[34] L.J. Fu, H.M. Yang, Tailoring the electronic structure of mesoporous spinel γ-Al₂O₃ at atomic level: cu-doped case, J. Phys. Chem. C 118 (2014) 14299–14315.

[35] Y. Zhang, Z. Liu, D. Zang, L. Feng, Structural and opto-electrical properties of Cu–Al–O thin films prepared by magnetron sputtering method, Vacuum 99 (2014) 160–165.

[36] F. Dong, Q. Li, Y. Zhou, Y. Sun, H. Zhang, Z. Wu, *In situ* decoration of plasmonic Ag nanocrystals on the surface of (BiO)₂CO₃ hierarchical microspheres for enhanced visible light photocatalysis, Dalton Trans. 43 (2014) 9468–9480.

[37] W. Luo, L.H. Zhu, N. Wang, H.Q. Tang, M.J. Cao, Y.B. She, Efficient removal of organic pollutants with magnetic nanoscaled BiFeO₃ as a reusable heterogeneous Fenton-like catalyst, Environ. Sci. Technol. 44 (2010) 1786–1791.

[38] C. Hammond, R.L. Jenkins, N. Dimitratos, J.A. Lopez-Sanchez, M.H. Rahim, M.M. forde, A. Thetford, D.M. Murphy, H. Hagen, E.E. Stangland, J.M. Moulijn, S.H. Taylor, D.J. Willock, G.J. Hutchings, Catalytic and Mechanistic insights of the low-temperature selective oxidation of methane over Cu-promoted Fe-ZSM-5, Chem. Eur. J. 18 (2012) 15735–15745.

[39] M.L. Kuznetsov, Y.N. Kozlov, D. Mandelli, A.J.L. Pombeiro, G.B. Shul'pin, Mechanism of Al³⁺-catalyzed oxidations of hydrocarbons: dramatic activation of H₂O₂ toward O–O homolysis in complex [Al(H₂O)₄(OOH)(H₂O₂)]²⁺ explains the formation of HO• radicals, Inorg. Chem. 50 (2011) 3996–4005.

[40] G. Zhang, J. Long, X. Wang, Z. Zhang, W. Dai, P. Liu, Z. Li, L. Wu, X. Fu, Catalytic role of Cu sites of Cu/MCM-41 in phenol hydroxylation, Langmuir 26 (2010) 1362–1371.

[41] P. Nieto, A. Günther, G. Berden, J. Oomens, O. Dopfer, IRMPD spectroscopy of metalated flavins: structure and bonding of Lumiflavin complexes with alkali and coinage metal ions, J. Phys. Chem. A 120 (2016) 8297–8308.

[42] Y. Wang, H. Zhao, G. Zhao, Iron-copper bimetallic nanoparticles embedded within ordered mesoporous carbon as effective and stable heterogeneous Fenton catalyst for the degradation of organic contaminants, Appl. Catal. B: Environ. 164 (2015) 396–406.